Arch Appl Mech
DOI 10.1007/s00419-016-1219-4

ORIGINAL

Gurmeet Singh · David Kumar · P. M. Mohite

Damage modelling of epoxy material under uniaxial tension based on micromechanics and experimental analysis

Received: 3 November 2016 / Accepted: 30 November 2016

Abstract Epoxy is a widely used thermosetting polymer in various engineering fields to develop composites. Studying its damage and fracture behaviour under various loading conditions is highly important. In this work, a micromechanics-based damage model is developed for understanding the damage initiation and growth in epoxy. To support this damage model, tests are performed for obtaining mechanical properties and to study the damage behaviour of epoxy. Diglycidyl ether of bisphenol A (DGEBA) resin with triethylenetetramine (TETA) hardener in 10:1 ratio are mixed and cured to make the epoxy. To give a physical meaning to damage, the model quantifies the damage as volume fraction of a spherical void in a unit representative volume element (RVE) of epoxy material. Degraded effective properties are computed for damaged RVE using standard mechanics-based micromechanical approach. A second-degree polynomial is established for effective stiffness with damage at any loading instance. This functional form of degraded stiffness in terms of damage is used in constitutive relations. A strain energy- based approach is used to compute thermodynamic forces, a state variable used for the evolution of damage. A damage evolution model is proposed with two material-specific parameters which are determined using experimental tests. The model is implemented by user material subroutine (UMAT) in commercial finite element software, Abaqus/Standard. The proposed model accurately captures the tensile behaviour of the epoxy material and gives capability to simulate an epoxy material's damage behaviour from its initiation till failure or macrolevel rupture under uniaxial tensile loading. The developed model predicts the behaviour of the material in agreement with experimental results.

Keywords Micromechanics · Damage model · Epoxy · Tensile test · Degraded stiffness

1 Introduction

Understanding the material failure mechanism and its modelling has always been important for the better utilization of materials in critical applications. Microlevel damage and macrolevel fracture have been the criteria to measure the degradation of material behaviour. Kachanov [1] and Rabotnov [2] in the past have shown that damage initiation is not the final fracture. Failure at microlevel grows with loading in the material and leads to macrolevel fracture. This process of damage involves degradation of the effective stiffness at those damaged material points. The continuum damage mechanics is the field which primarily deals with it

G. Singh · D. Kumar · P. M. Mohite (✉)
Department of Aerospace Engineering, Indian Institute of Technology, Kanpur, Uttar Pradesh 208016, India
E-mail: mohite@iitk.ac.in
Tel.: +91 5122596024

G. Singh
E-mail: chdgurmeet@gmail.com

D. Kumar
E-mail: david@iitk.ac.in

Published online: 30 December 2016

[3]. Janson [4] in his work has demonstrated how microlevel damage leads to macrolevel fracture. Mazars and Pijaudier-Cabot [5], assumed some microlevel damage and fracture variables and established some relations between them using thermodynamics.

Damage in a material is referred as discontinuities in continuum, and it is represented as the creation and growth of microvoids in the continuum. Damage, in its physical sense, is always related to inelastic or irreversible strains and more generally to strain energy dissipation which occurs either on the mesoscale (the scale of the RVE), or on the microscale, the scale of the discontinuities. Ladevèze et al. [6–8] used damage mechanics and thermodynamics principles to predict the progressive damage in interlaminar interface and growth of fracture. They used state-dependent variables to compute the deterioration of material and damage initiation and its evolution. They used a linear degradation of the stiffness with damage from its initiation to failure at macrolevel. Different damage parameters were used for failure modes in the damage modelling of the composites. The numerical methods developed by Ladevèze [9,10] in prediction of rupture enhanced the computational capabilities in computational damage mechanics.

In this study, a novel model is developed to explain the damage initiation and its growth for polymer materials. Standard mechanics-based micromechanical approach is used to compute effective properties of a representative volume element (RVE) [11]. For modelling the damage, an RVE with a spherical void at its centre is considered. The spherical void is assumed to have no elastic properties and rest of the material is given the properties of an epoxy material. The volume fraction of the spherical void is the measure of damage in the RVE. Effective elastic properties of the RVE for a series of damage sizes are computed using standard mechanics approach known as Hill's concentration factor approach [11,12]. A quadratic relation is established for degraded elastic properties and the damage indicator.

For establishing a damage law including damage initiation and damage saturation strain energy release rate with respect the damage is used. A simple inelastic strain model is used in terms of damage and ultimate fracture strain of the material. A general form of damage evolution is established, and then a material-specific damage law is obtained by best matching computation stress–strain behaviour with the experimental one. This model is implemented using user material subroutine in Abaqus/Standard [13,14]. Abaqus/Standard offers a platform to define a user's choice constitutive relation using user material subroutine [14].

Material under this study is epoxy. This is the mostly used polymeric material in aerospace applications. Various composites, such as nanocomposites [15–17], glass fibre/epoxy [18,19], carbon fibre/epoxy [20–25], have been developed using this material. It has excellent binding properties and provides great matrix behaviour. It transfers the load to the reinforcing fibres without any lag. Performing its damage analysis is very important to enhance the design capabilities of the composite materials. In this work, epoxy system constitutes diglycidyl ether of bisphenol (DGEBA) resin and triethylenetetramine (TETA) hardener. Experimental study is conducted for mechanical properties of this epoxy. Experimentally obtained data is used for the user material subroutine as input which gives the damage evolution model parameters for this material.

In the following the micromechanical modelling of damage, its modelling and experimental evaluation are presented.

2 Micromechanical modelling of damage

Micromechanics is widely used to determine the effective properties of the materials such as composites and solid foams. consists of two or more constituents of different properties and distribution. In a fibrous composite at the fibre and matrix level, it is used to determine the effective or averaged elastic or inelastic properties of a composite lamina, depending on the distribution, properties and volume fraction of each constituents in the RVE. The following section will describe the definition of the damage and its micromechanical model developed in the present work.

2.1 Damage: definition and quantification

Many researchers in the past have modelled different modes of damage at micro or continuum level using micromechanics. For example, Chevalier et al. [26] have modelled the damage in an RVE and analysed it using micromechanics. Furthermore, based on this study, they proposed a new fracture criterion for semi brittle epoxy materials. They considered the defect as ellipsoidal void in an RVE. In the present study, the progressive internal deterioration of the material is represented by a single spherical void inside an RVE. The radius of the sphere r increases as the progressive material degradation occurs, as shown in Fig. 1. The change

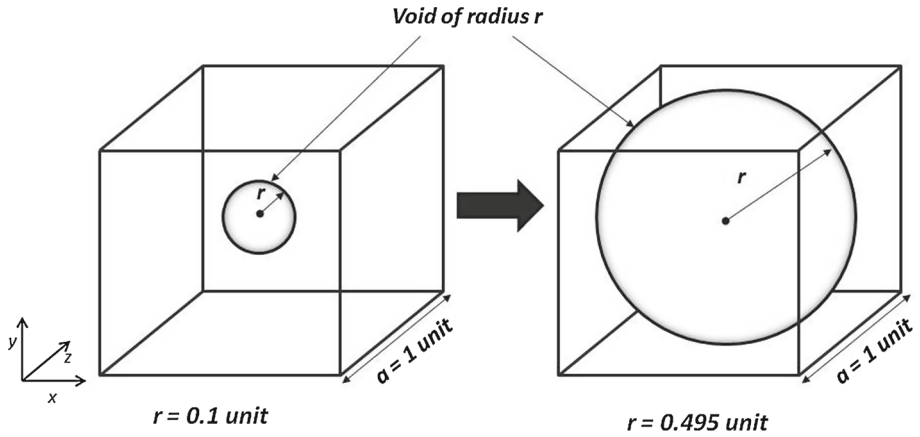

Fig. 1 Growth of void or damage in an RVE

in state of stress or strain leads to change in spherical void in the RVE which, in turn, leads to degradation of the elastic behaviour of the material. The damage d is quantified as the volume fraction of the spherical void in the RVE is given as:

$$d = \frac{V_{\text{VOID}}}{V_{\text{RVE}}} \tag{1}$$

where, V_{VOID} and V_{RVE} are volume of the void and RVE of side a, respectively, and are defined as follow: $V_{\text{VOID}} = \frac{4}{3}\pi r^3$; $V_{\text{RVE}} = a^3$. In the computations $a = 1$, is taken. Micromechanical analysis is performed on this RVE for various damage sizes for computations of the effective properties of the RVE using Hills concentration factors approach [11,12] which is briefly explained in the next section.

Damage initiation can be visualized as the sprouting of the spherical void in the unit cube. It is assumed that there will be no damage in the material till it reaches yield stress during its loading history. After reaching yield once, as stress grows further, it leads to growth of the void and hence the damage value increases till final fracture. In a unit cube RVE, due to computational constraints, the allowable value of damage size is from $r = 0$ to $r = r_c = 0.495$ units. As void grows to r_c, the damage d becomes critical (d_c). At d_c, the damage reaches saturation and RVE breaks completely. This stage is the start of macro level material fracture in the body. It is to be noted that in continuum, an RVE represents a point.

2.2 Hill's concentration factors approach

Micromechanics employs different methods to compute the averaging of the properties. Gregy [27] in his work has shown that the mathematical theory of homogenization [28] and Hill's concentration factors approaches [11,12] yield similar results for an RVE with spherical void at its centre. In this study, Hill's concentration factor approach is used to compute the effective properties of the RVE with void and matrix as its constituents. This standard mechanics-based approach works on the principle of stress and strain averaging in a composite material with fibre and matrix as two phases [11]. The average strains as a linear combination of unit strains were applied on RVE boundary surfaces. Thus, six fundamental cases were analysed state of strains and stress in the phases. The void has a volume fraction for each size of its radius and has zero elastic properties. The averaged stresses $\bar{\sigma}_{ij}$ in the RVE related to corresponding average strains $\bar{\epsilon}_{kl}$ applied, are given as:

$$\bar{\sigma}_{ij} = \left[V_v C^{(v)}_{ijpm} \bar{A}^{(v)}_{pmkl} + V_m C^{(m)}_{ijpm} \bar{A}^{(m)}_{pmkl} \right] \bar{\epsilon}_{kl} = C^*_{ijkl} \bar{\epsilon}_{kl} \tag{2}$$

where subscripts v and m represent the quantities correspond to void and matrix material, respectively. V is the volume fraction, C_{ijpm} is stiffness of the phase, $\bar{A}_{pmkl}$ is the phase averaged Hill's strain concentration factor and C^*_{ijkl} represents the effective stiffness of the RVE. The details of this method can be seen in [11,29]. Hence, for computing effective properties of the RVE of various void volume fractions, the void is assigned zero stiffness, i.e. $C^{(v)}_{ijpm} = 0$. Now, Eq. (2) can be rewritten as:

$$\left[V_m C^{(m)}_{ijpm} \bar{A}^{(m)}_{pmkl} \right] \bar{\epsilon}_{kl} = C^*_{ijkl} \bar{\epsilon}_{kl} \tag{3}$$

Hill [11,12] introduced the pointwise phase concentration factors to relate the pointwise strains with its phase averaged values. These concentration factors can be averaged over its own phase to give averaged values as:

$$\bar{A}^{(m)}_{ijkl} = \frac{1}{V_m}\int_{V_m} A^{(m)}_{ijkl}(\mathbf{x})dV_m \tag{4}$$

Using this phased averaged strain concentration factor, phase averaged pointwise strains in epoxy material $\bar{\epsilon}^{(m)}_{ij}$ can be related to RVE averaged strain $\bar{\epsilon}_{kl}$ as follow:

$$\bar{\epsilon}^{(m)}_{ij} = \bar{A}^{(m)}_{ijkl}\bar{\epsilon}_{kl} \tag{5}$$

$$\bar{\epsilon}^{(m)}_{ij} = \frac{1}{V_m}\int_{V_m} \epsilon^{(m)}_{ij}(\mathbf{x})dV_m \tag{6}$$

here, $\bar{A}^{(m)}_{ijkl}$ is obtained by applying uniform strains on the RVE in Abaqus/Standard. Six different uniform strains as displacement ($\bar{\epsilon}_{kl}$) are applied and $\epsilon^{(m)}_{ij}(\mathbf{x})$ are pointwise strain fields obtained from the FEM solution. These strain fields are averaged over the whole volume of the RVE using Eq. (6). Bar on the deformation symbols indicates the averaged value over the RVE. Therefore, all rows of $\bar{A}^{(m)}_{ijkl}$ are obtained by six uniform boundary conditions applied on the particular RVE. Hence, for various values of V_m, the degraded effective stiffness matrix C^*_{ijkl} of the RVE is obtained from this micromechanical analysis. In this study, Young's modulus and Poisson's ratio of the epoxy material are obtained from tensile testing. These values are fed as RVE material for the micromechanical analyses. Various radii of the spherical damage are considered and damaged elastic constants are evaluated using Eq. (3). Then to use this effective stiffness in a progressive damage model, a second-order regression models are fit for elastic constants and damage (d) as follow.

$$E_d = E_0\left(1 + E_1 d + E_2 d^2\right) \tag{7}$$

$$\nu_d = \nu_0\left(1 + \nu_1 d + \nu_2 d^2\right) \tag{8}$$

$$G_d = G_0\left(1 + G_1 d + G_2 d^2\right) \tag{9}$$

where subscripts 0 and d refer to undamaged and damaged value of elastic constants, respectively. As evident from the equations, subscripts 1 and 2 are the coefficients for that elastic constant in the second-order regression fit equation. These coefficients will be obtained by carrying out micromechanical analyses of the unit RVEs with various void sizes. These equations will be used in the damage evolution model for energy released rate computations and stiffness matrix update.

3 Progressive damage evolution model

A damage evolution model defines the growth of damage from its initiation to its saturation. Damage starts after a threshold at a material point and its growth needs to be defined in terms of state-dependent variables which can be quantified at every material point at any instant of loading till the damage saturates and a macro level fracture initiates. In this study, damage growth is described in terms of a thermodynamic force or energy release rate which is a state-dependent function and computed using strain energy.

3.1 Strain energy density and damage force

Strain energy density is the elastic energy stored per unit volume by a material under loading. At any point in a loaded material, the strain energy density U_0 is given by:

$$U_0 = \frac{1}{2}\sigma_{ij}\epsilon_{ij} \tag{10}$$

This strain energy density can be split into hydrostatic strain energy U_H and distortional stain energy U_D as:

$$U_0 = \frac{\sigma_H^2}{2K} + \frac{\sigma_{\mathrm{VM}}^2}{6G} \tag{11}$$

where, σ_H is hydrostatic stress component and σ_{VM} is von Mises stress component developed at a material point. The von Mises stress is evaluated from the deviatoric stress component of the stress tensor as:

$$\sigma_{VM} = \sqrt{\frac{3}{2}\sigma_{ij}\sigma_{ij}} \tag{12}$$

Hence, distortional stain energy U_D is:

$$U_D = \frac{\sigma_{ij}\sigma_{ij}}{4G} \tag{13}$$

However, hydrostatic component of the state of stress is evaluated as follow:

$$\sigma_H = \frac{1}{3}tr(\sigma_{ij}) = \frac{\sigma_{kk}}{3} = \frac{\sigma_{11}+\sigma_{22}+\sigma_{33}}{3} \tag{14}$$

In case of metals, the hydrostatic state of stress does not affect the yield behaviour. However, as shown by Ward [30] for polymers, the yield stress and nonlinear behaviour are affected by the hydrostatic stress. Pan et al. [31,32] and Hsu et al. [33] have explained the effects of hydrostatic stress component by including into their visco-plasticity models using the variation of the Drucker–Prager yield criterion [34]. Hydrostatic stress σ_H can be compressive or tensile, and hence, it is important to note the effect of compressive σ_H on damage. In case of resins, the compressive hydrostatic stress plays a significant role to maintain the continuity of the material, and it does not allow growth of the damage in the material, rather it closes the void at micro level. So, to incorporate this effect, Eq. (11) is modified and rewritten as:

$$U_0 = \frac{\langle\sigma_H\rangle_+^2}{2K_d} + \frac{\langle\sigma_H\rangle_-^2}{2K_0} + \frac{\sigma_{VM}^2}{6G_d} \tag{15}$$

where, K_0 is undamaged bulk modulus and K_d and G_d are damaged bulk and shear moduli, respectively. Here, $\langle\rangle_+$ and $\langle\rangle_-$ are evaluated in case of tensile σ_H and compressive σ_H, respectively. This operator indicates that the damage will grow when the hydrostatic stress is tensile in nature. However, when the hydrostatic stress is compressive in nature then the damage remains same. K_0, K_d and G_d can be computed in terms of damaged Young's modulus and Poisson's ratio at any damaged state as:

$$K_d = \frac{E_d}{3(1-2\nu_d)};\ K_0 = \frac{E_0}{3(1-2\nu_0)};\ G_d = \frac{E_d}{2(1+\nu_d)} \tag{16}$$

here, subscript d and 0 represent the damaged and undamaged values of mechanical constants, respectively. Damaged elastic constant will be evaluated from the micromechanical analysis of the damaged RVE.

3.2 Damage evolution model

The thermodynamic force or damage force Y_d associated with damage d is calculated as the rate of change of strain energy density with respect to damage d at the loading step corresponding to τ is given as:

$$Y_d^\tau = -\frac{\partial U_0}{\partial d} \tag{17}$$

where $(-)$ sign signifies the energy dissipated out of the system. Damage initiates when a material yields or von Mises stress reaches yield stress of the material. This is true for metals but to account for the effect of hydrostatic stresses in resin, damage initiation criterion is defined using damage force. The corresponding value of damage force is referred as threshold damage force, Y_0. Hence, putting the values of tensile yield stress σ_y^t and compressive yield stresses σ_y^c and Y_d is computed with $d = 0$ to give Y_0. Similarly, damage saturation reaches when damage force reaches its critical value Y_c and damage d attains its maximum value, d_c and RVE breaks at this stage. Hence, the material fails at this point. The value of Y_c is computed by putting ultimate stress in tension σ_{ult}^t as well as in compression σ_{ult}^c of the material along with $d = dc$ in the expression of Y_d in Eq. (17). In the proposed evolution model, the healing of the damage is not considered. Here, only growing nature of the damage is modelled. This is done by taking a maximum value of the thermodynamic force at a given material point until the current loading state. Thus, $Y_d = \max_{0\le\tau\le t} Y_d^\tau$.

For evaluating inelastic strains at a damaged state, a linear inelastic strain model is defined. Inelastic strain $\epsilon_{d_{ij}}^{IN}$ at any damaged state is calculated in terms of damage d, d_c and failure strain of the material as:

$$\epsilon_{d_{kl}}^{IN} = \epsilon_{d_{ckl}}^{IN} \left(\frac{d}{d_c} \right) \tag{18}$$

where $\epsilon_{d_{ckl}}^{IN}$ is the inelastic strain in tensorial form at $d = d_c$, which is essentially the fracture strain or ultimate strain of the material. This inelastic strain is related to stress at any stage between $d = 0$ to $d = d_c$ as follows:

$$\sigma_{ij}^{d} = C_{ijkl}^{d} \epsilon_{kl}^{e} = C_{ijkl}^{d} \left(\epsilon_{kl} - \epsilon_{d_{kl}}^{IN} \right) \tag{19}$$

where, C_{ijkl}^{d}, ϵ_{kl}^{e} and ϵ_{kl} are degraded stiffness, elastic strain tensor and total strain tensor in the material at any loading stage, respectively. The 3D constitutive relation of elastic strain and stress in terms of damaged E_d and ν_d at a material is given in the following equation:

$$\begin{pmatrix} \epsilon_{11}^{e} \\ \epsilon_{22}^{e} \\ \epsilon_{33}^{e} \\ \gamma_{23}^{e} \\ \gamma_{13}^{e} \\ \gamma_{12}^{e} \end{pmatrix} = \begin{bmatrix} \frac{1}{E_d} & \frac{-\nu_d}{E_d} & \frac{-\nu_d}{E_d} & 0 & 0 & 0 \\ \frac{-\nu_d}{E_d} & \frac{1}{E_d} & \frac{-\nu_d}{E_d} & 0 & 0 & 0 \\ \frac{-\nu_d}{E_d} & \frac{-\nu_d}{E_d} & \frac{1}{E_d} & 0 & 0 & 0 \\ 0 & 0 & 0 & \frac{2(1+\nu_d)}{E_d} & 0 & 0 \\ 0 & 0 & 0 & 0 & \frac{2(1+\nu_d)}{E_d} & 0 \\ 0 & 0 & 0 & 0 & 0 & \frac{2(1+\nu_d)}{E_d} \end{bmatrix} \begin{pmatrix} \sigma_{11} \\ \sigma_{22} \\ \sigma_{33} \\ \tau_{23} \\ \tau_{13} \\ \tau_{12} \end{pmatrix} \tag{20}$$

This stress is used to calculate Y_d, which determines the value of damage in the material at this state of stress. Following the work by Ladevèze et al. [8], a damage evolution model is proposed as:

$$d = \begin{cases} d = 0 & \text{when } Y_d < Y_0 \\ d = d_c \left[\dfrac{Y_d^m - Y_0^m}{Y_c^m - Y_0^m} \right]^n & \text{when } Y_0 \leq Y_d \leq Y_c \\ d = d_c & \text{when } Y_0 \leq Y_d \leq Y_c \end{cases} \tag{21}$$

where m and n are material-specific parameters which depend on the material under study. These coefficients are obtained using best curve fitting on experimental stress strain curve for a uniaxial tensile test. Experiments are carried out to evaluate properties like Young's modulus, Poisson's ratio, yield stress, and ultimate stress along with stress–strain curve of neat epoxy material.

Different values of m and n are taken in the evolution model for a material under study. Then material parameters, m and n will be obtained using the best matching computed stress strain curve with experimental stress strain curve. These values of m and n in evolution model can be used to describe the behaviour of the actual material in a computational model implemented in Abaqus/Standard using user material subroutine (UMAT) [14]. The algorithm followed in the study is presented in Fig. 2. UMAT requires input parameter in the user defined material section of ABAQUS/Standard. The algorithm starts with taking some ith state stress components from the solver. Using these stress components, it evaluates the σ_H and proceeds accordingly with the usage of damage or undamaged bulk modulus value. Then thermodynamic forces are evaluated and the damage is calculated according to threshold value of these forces and damage is further evolved.

4 Experimental study

The proposed damage model needs elastic moduli and strength parameters evaluated from experimental study for the material chosen. Here, epoxy material is prepared and tested for its tensile properties. The details of the experimental testing procedure to evolve their moduli and strength parameters along with material development are presented in the following subsections.

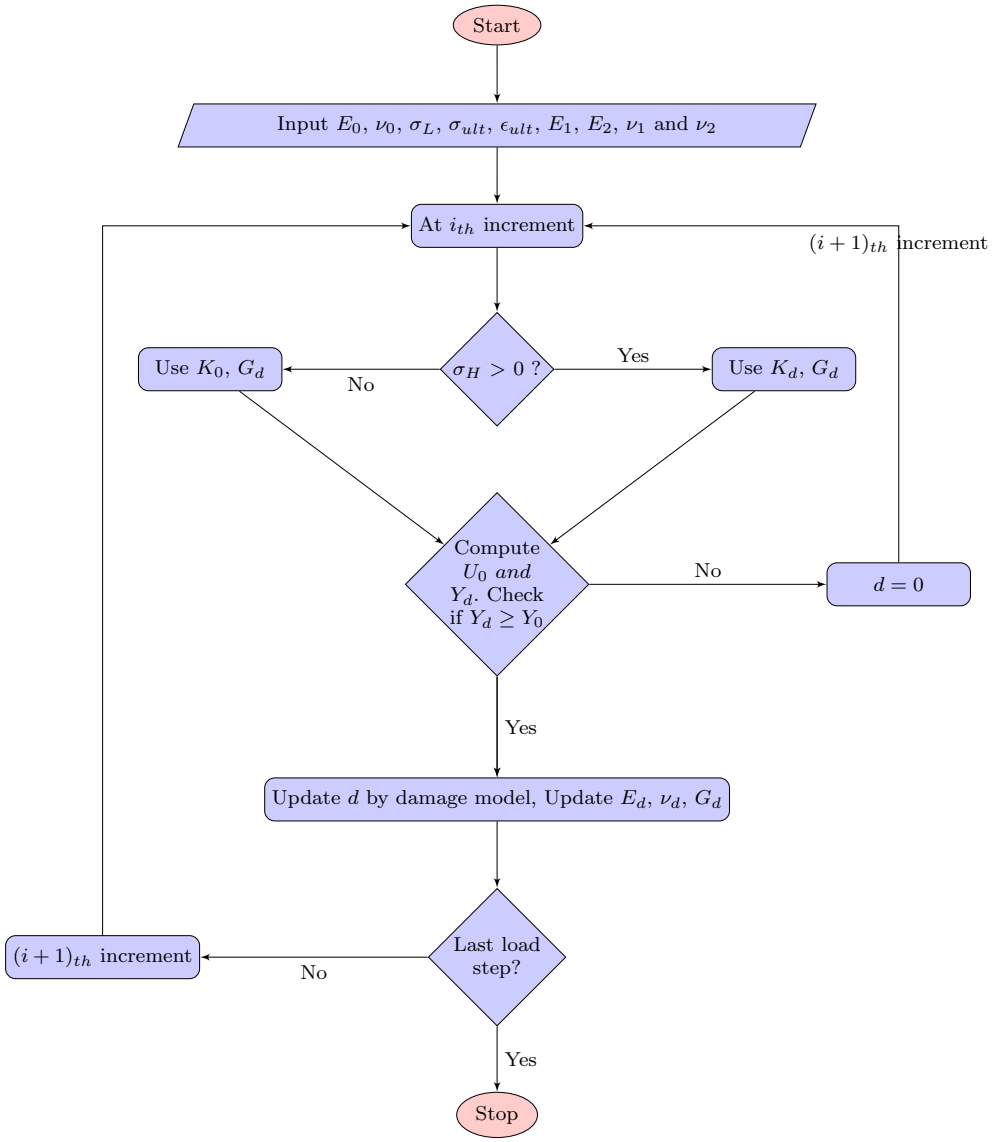

Fig. 2 Flowchart for UMAT algorithm

4.1 Material development

Epoxy system, which constitutes diglycidyl ether of bisphenol (DGEBA) resin and triethylenetetramine (TETA) harder, is used in this study. Montazeri et al. [35] studied the effect of curing cycle on the mechanical properties of neat epoxy and multi-walled carbon nanotubes (MWCNTs)/epoxy composites. They used two curing cycles: The first was heating at 80 °C for 4 h and the second was curing at room temperature for 24 h followed by 4 h heating at 80 °C. The properties for the second curing process were better than the first one, second curing process is followed in current study. ASTM D638 designation is used for finding tensile properties of reinforced and unreinforced plastics [36]. Epoxy samples are prepared using a mould which constitutes an aluminium plate with 10 samples shape cut outs as shown in Fig. 3 and two steel plates to cover this cut outs plate from both sides. Special attention was paid in the manufacturing of the mould to achieve the specimen with same dimensions. CNC machine was used to manufacture the mould. A CAD model based on ASTM standard geometry was developed and fed to the machine during manufacturing process.

The resin and hardener are mixed in 10:1 ratio. Following procedure is used for making the specimen.

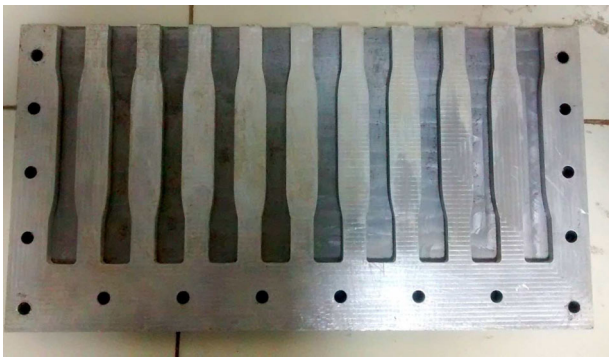

Fig. 3 Mould for making epoxy tensile testing specimen

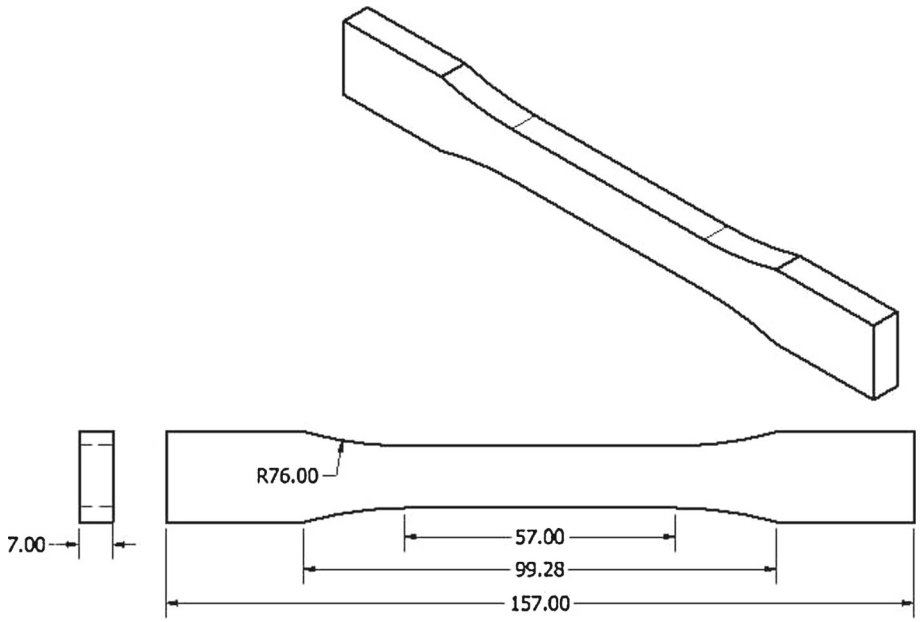

Fig. 4 Tensile testing specimen dimensions

1. Pour the hardener into resin beaker gently near to the wall of the beaker to prevent air bubbles during pouring and stir it for 8–10 min.
2. Pour the mixture into the mould cavities gently and keep it at 34 °C (room temperature) for 24 h in oven at atmospheric pressure.
3. After 24-h cycle, increase the oven temperature to 80 °C and keep it for 4 h.
4. Let the temperature of the mould sets down to room temperature gradually and then remove the plates of the mould. Then remove the samples out of it.

The dimensions of a specimen are shown in Fig. 4. All the dimensions mentioned in the figure are in mm.

4.2 Material testing

Experimental testing of prepared epoxy specimen under uniaxial tension is carried out using Tinius Olsen UTM of 10 KN capacity. Longitudinal strain in the middle section of the specimen is measured using an extensometer of 25 mm gauge length. For obtaining the Poisson's ratio, strains for longitudinal and lateral directions are required. Installing two extensometers on a sample was not possible; therefore, two strain gauges were pasted along longitudinal and transverse directions on the sample. Soldering on both the strain gages was done to receive the data. For measurement of strain from strain gauges, National Instruments NI 9923 strain module is used. The connections of both strain gauges are made in half bridge mode for data acquisition. Longitudinal

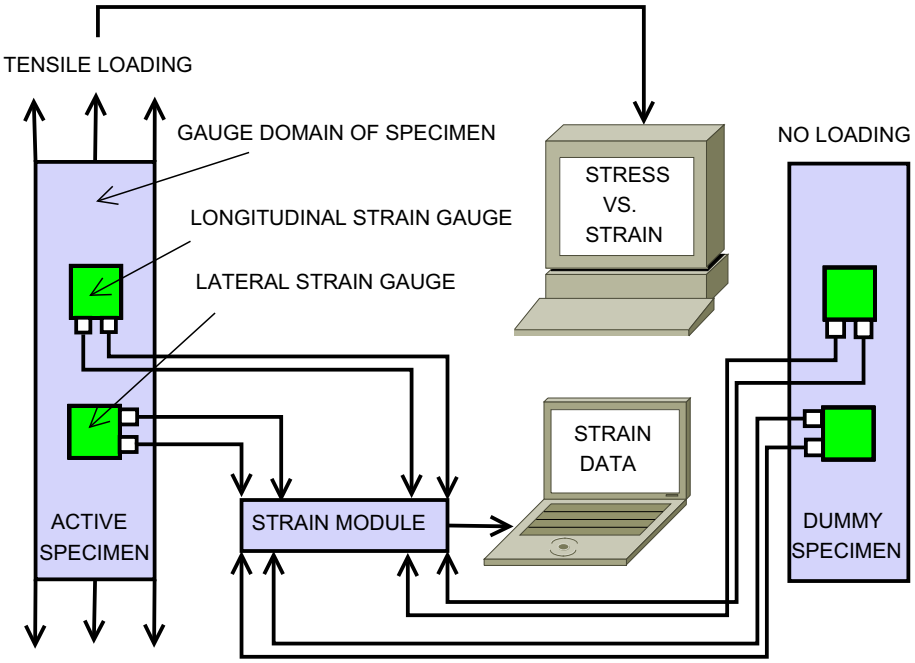

Fig. 5 Tensile testing set-up for stress and strain measurements

and transverse strain gauge connections are made in two different channels and both read values relative to their counterparts embedded on a dummy sample which is not under load. Complete experimental set-up is shown in Fig. 5. A LabVIEW program developed for measurement of Poisson's ratio, is used for data acquisition. The quasi-static strain rate is considered as $10^{-5}/s$ [37] and it was used by Gilat et al. as well in [38]. The gauge length of the epoxy samples is 50 mm. Thus, the cross head speed chosen is 0.03 mm/min [36].

5 Results and discussion

In this section, the results obtained from experimental testing and the micromechanical analysis of an RVE with spherical void damage in it, are presented.

5.1 Experimental results

Epoxy samples are tested at quasi-static loading on Tinius Olsen UTM. The cross head speed for quasi-static loading is set to 0.03 mm/min. The gauge length of the epoxy samples is 50 mm, so the strain rate is $10^{-5}/s$. Young's modulus, limit of linearity, ultimate stress, and ultimate strain are evaluated for all tested samples. In this work, five samples are tested to take into account the variability and to get consistency in results. Stresses are calculated using the load given by UTM machine and the original cross sectional area of the sample while, longitudinal strain is obtained from extensometer. This stress and longitudinal stain are used to compute Young's modulus and other points on stress vs. strain curve. However, Poisson's ratio is evaluated from the strain data obtained from longitudinal and transverse strain gauges. The properties obtained for all specimen are shown in Table 1.

Averaged value of Young's modulus of all specimens under study is 3.566 GPa. The Young's modulus is obtained in the initial linear region of the curve by least square fitting with the value of $R^2 \geq 0.98$. Poisson's ratio is consistent for all tests with very slight deviation and average value is 0.3734. Average value of linearity limit is 25.06 MPa, average ultimate stress value is 50.18 MPa, and ultimate or fracture strain is 1.723%. Stress vs. strain curves for all test cases together are shown in Fig. 6.

The obtained results for an epoxy material are in good agreements in literature [38]. Further, the very low values of standard deviation (SD) show that the tests are repeatable.

Table 1 Material properties of epoxy obtained by testing

S. No	E (GPa)	Linearity limit (MPa)	σ_{ult} (MPa)	ϵ_{ult}	ν
1	3.6178	25.12	49.84	0.0160	0.3738
2	3.3793	24.53	47.80	0.0173	0.3723
3	3.6213	23.65	51.32	0.0174	0.3744
4	3.6126	25.42	51.21	0.0190	0.3735
5	3.5995	26.60	50.73	0.0165	0.3728
Mean	3.5661	25.06	50.18	0.0173	0.3734
SD (%)	2.94	4.35	2.89	6.38	0.21

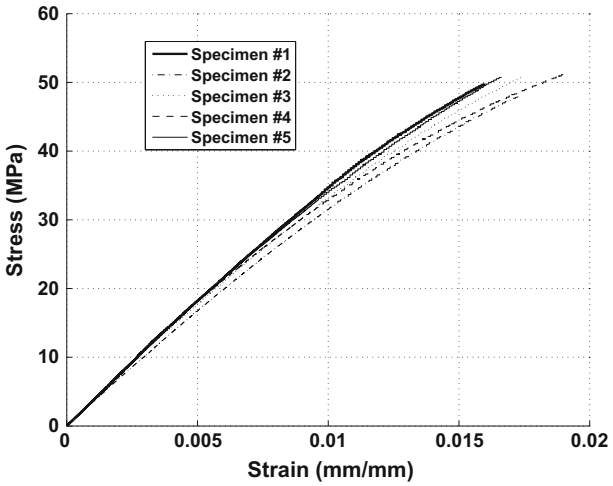

Fig. 6 Stress-Strain behaviour of all epoxy Specimens

5.2 Micromechanical analysis

Elastic properties of epoxy resin DGBEA/TETA in undamaged state are as obtained by tests and presented in previous subsection. The micromechanical analysis is carried out for void radii $r = 0.1, 0.2, 0.3, 0.35, 0.4, 0.45, 0.48$ and 0.495 unit of the spherical void. The von Mises stress plot of the RVE under uniform strain along z on the boundary of the RVE for some of these radii are shown in Fig. 7. Similarly, other five uniform strains are applied as boundary conditions on the outer surface of every RVE. Applying uniform strains ($\bar{\epsilon}_{kl}$) as boundary conditions, give rise a strain field ($\epsilon_{ij}^{(m)}$) in the RVE. Individuals components of the strains are averaged ($\bar{\epsilon}_{ij}^{(m)}$) over the RVE and the averaged strain concentration factor ($\bar{A}_{ijkl}$) is computed using Eq. (5). Hence, using averaged strain concentration factors, effective stiffness of the RVE is obrained using Eq. (3).

Corresponding to these void radii, the effective properties of the RVE are obtained. A 2nd degree polynomial is fit between effective properties and damage d. Variation of Young's modulus, Poisson's ratio, and shear modulus with damage parameter are shown in Figs. 8, 9 and 10, respectively. Furthermore, the second-degree polynomial curve fitting is also shown in figures. The robustness for these fittings are more than 0.999.

It can inferred from the degraded elastic constants curves that Young's modulus and shear modulus decrease with quite high rate with increase in damage. While, Poisson's ration shows lesser sensitivity with increase in the damage size inside the RVE.

To implement in a progressive damage model, it is necessary to write these data points in a continuous functional form which is used in strain energy equations. Further, this is then used for the computation of damage force and hence damage parameter itself for a new state of stress. The fitted quadratic curves for elastic degradation are given by following equations.

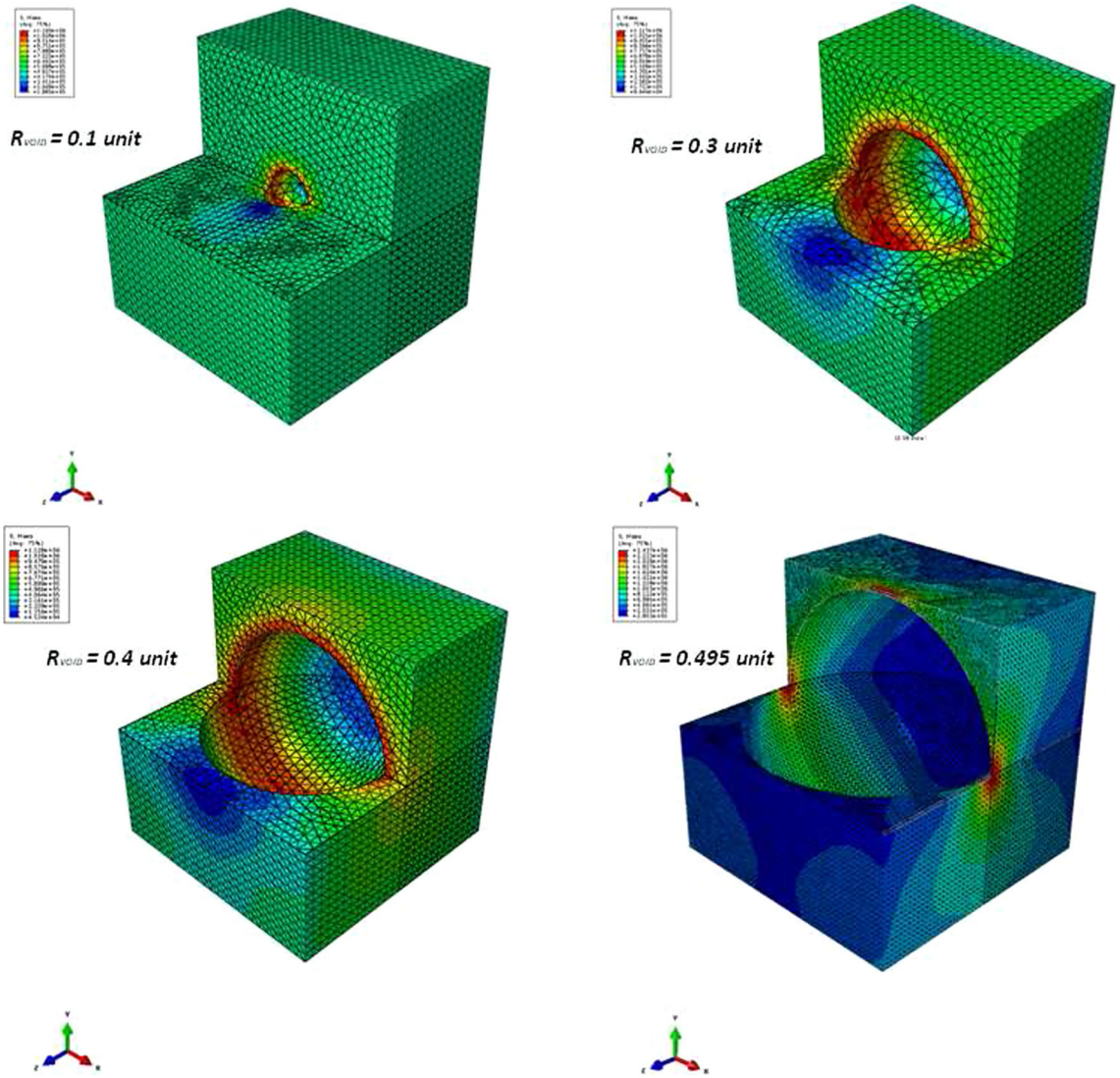

Fig. 7 von Mises stress for different void radii RVEs in cut view

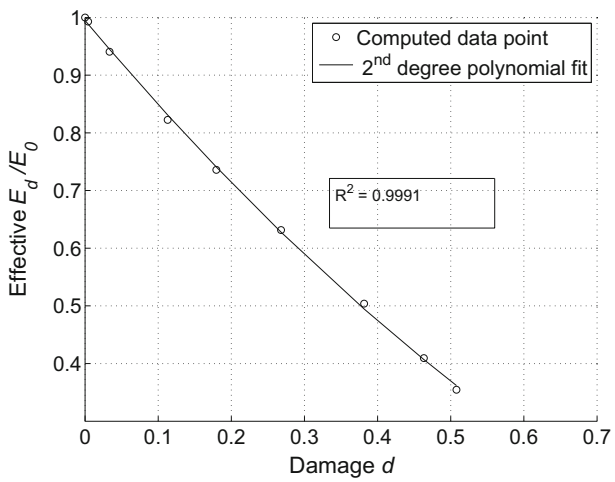

Fig. 8 Variation of Young's modulus with damage

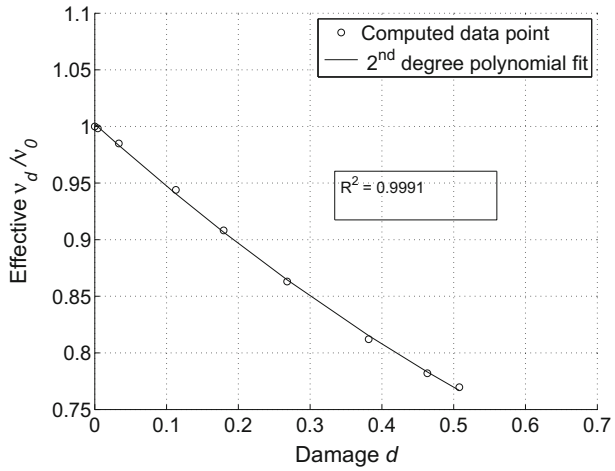

Fig. 9 Variation of Poisson's ratio with damage

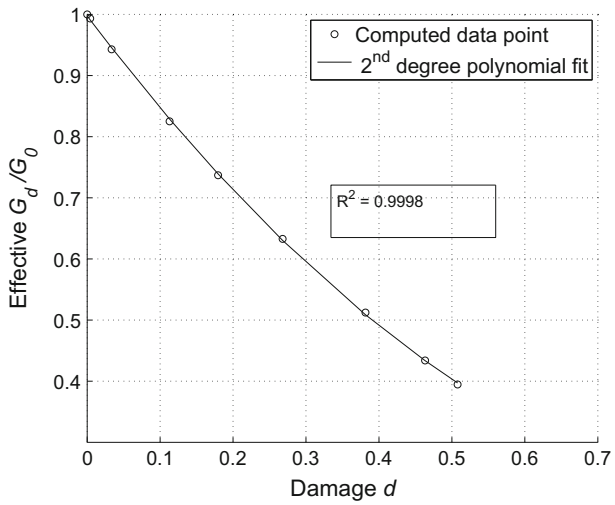

Fig. 10 Variation of shear modulus with damage

$$E_d = E_0\left(0.514d^2 - 1.507d + 0.9948\right) \tag{22}$$

$$\nu_d = \nu_0\left(0.210d^2 - 0.570d + 1.0022\right) \tag{23}$$

$$G_d = G_0\left(0.785d^2 - 1.581d + 0.9975\right) \tag{24}$$

The maximum radius of the spherical void that can be included inside an RVE of unit size is 0.495 unit. A shown in Fig. 7, the RVE with this radius of damage has very refined mesh. Increasing the size of the further will lead to very thin elements in the middle of each face. Such a implementation in FE model will require to further refinement in mesh and hence will increase computational complexity in the implementation using Abaqus/Standard. This size of void corresponds to complete fracture of the RVE. Therefore, the critical damage parameter d_c, corresponding to this void size is 0.508.

5.3 Damage evolution model for epoxy

For describing the damage in a material from its initiation to final failure, damage evolution model is essential to be defined. This governs the material behaviour after damage initiation. In this work, the damage evolution is given in terms of thermodynamic force, as defined in Sect. 3.2. The material constants in the proposed damage model for epoxy are obtained by computational tensile tests carried out using user material subroutine

Table 2 Input to Abaqus/Standard for UMAT

Input	Value
Young's modulus (E_0)	3566 MPa
Poisson's ratio (ν_0)	0.37
Linearity limit (σ_L)	25.06 MPa
Ultimate stress (σ_{ult})	50.18 MPa
Ultimate strain (ϵ_{ult})	0.0173
Coefficient of d in E_d (E_1)	−1.507
Coefficient of d^2 in E_d (E_2)	0.514
Coefficient of d in ν_d (ν_1)	−0.570
Coefficient of d^2 in ν_d (ν_2)	0.210

(UMAT) in Abaqus/Standard. The inputs of UMAT are the material properties obtained from experimental testing and micromechanical analysis of the RVE with various damage sizes. These material properties of epoxy are fed into the UMAT to run multiple simulations on a tensile test specimen in Abaqus/Standard to obtain the material-specific parameters of proposed damage model. The full list of the properties required as input to computational test, are mentioned in Table 2.

In actual specimen, when the stress reaches maximum value and strain reaches to its ultimate value, the material fails completely. It simply means that there is no stiffness at those points which reach to these critical values. Therefore, to capture this phenomenon in this damage model computationally, a condition on stiffness is applied. As soon as the damage d in an element reaches it's critical value, the stiffness of that material point is forced to reduce to a very small value and there would be a sharp drop in stiffness value. After this point onward, that element will continue to stretch but will carry no or very small stress. Thus, the set of failed elements will not have enough stiffness to resist deformation. This is the initiation of a macrolevel crack, and it can grow further if neighbouring elements of the failed region are also not capable of sustaining load. This is the growth of the macro level crack. After carrying out computations on tensile test for epoxy, $m = 2.0$ and $n = 0.75$ are the obtained values of the material parameters which can describe the best material behaviour. For these material parameters, the damage model for the epoxy under consideration can be described as:

$$d = \begin{cases} 0 & \text{when} \quad Y_d < Y_0 \\ d_c \left[\dfrac{Y_d^2 - Y_0^2}{Y_c^2 - Y_0^2} \right]^{0.75} & \text{when} \quad Y_0 \le Y_d < Y_c \\ d_c & \text{when} \quad Y_c \le Y_d \end{cases} \tag{25}$$

This damage model can be implemented in Abaqus/Standard using UMAT subroutine for any structural component of epoxy material.

A flat specimen of 10 mm × 5 mm × 100 mm is simulated for computational tensile test. Finite element model is developed using 15534 quadratic tetrahedral elements of type C3D10 of Abaqus/Standard with second-order accuracy. An axial displacement loading is applied at the ends of the specimen. The geometric model along with boundary conditions is shown in Fig. 11. The computed stress–strain curve by using this model along with all the experimental curves, are shown in Fig. 12. From this figure, it is clearly seen that the axial stress-strain curve predicted from the proposed model captures the experimental curves very accurately. The properties from the computational curve like Young's modulus, σ_{ult} and ϵ_{ult} are 3.57 GPa, 51.97 MPa and 0.0173, respectively. These values are in agreement with those obtained from experimental tests.

6 Conclusions

In this study, a micromechanics-based damage model is developed for DGBEA/TETA epoxy material. A micromechanics model based on standard mechanics with displacement loading is used to model a damage in an RVE and to compute damaged or degraded effective properties of the epoxy resin. Experimental tests are carried out to obtain elastic constant and strength parameter for axial tensile loading of this epoxy at quasi-static strain rate. A damage evolution model is proposed in terms of thermodynamic force with two material-specific parameters. The constitutive model is implemented in Abaqus/Standard by means of user material subroutine.

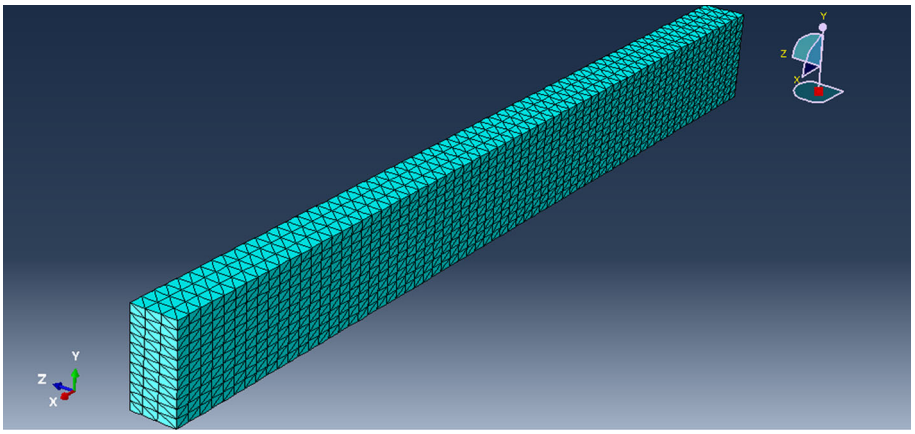

Fig. 11 Tensile specimen FEM model in Abaqus/Standard

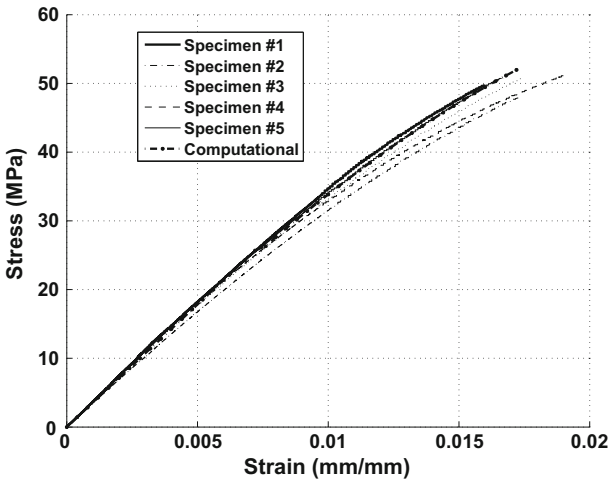

Fig. 12 Computational and experimental stress vs strain curves

The experimentally determined mechanical properties are used as input to the micromechanics model to predict degraded properties corresponding to various damage sizes in the RVE and damage evolution model material parameters. The major points from this study that can be concluded are as follows:

1. The stiffness of an RVE with damage shows an isotropic nature. The degraded elastic constants vary quadratically in terms of damage parameter.
2. Averaged mechanical properties of DGBEA/TETA Epoxy at quasi-static strain rate, are obtained from experimental tests: The average Youngs modulus is 3.57 GPa, Poissons ratio is 0.37, and shear modulus is 2.60 GPa. The ultimate tensile strenth is 50.18 MPa and ultimate strain is 0.0173. The standard deviation in these measured quantities is maximum of 6.38 %.
3. The axial tensile stress–strain curve for all tests carried out are close to each other. This indicates the repeatability of the material preparation and testing procedure followed.
4. The damage evolution model parameters are obtained from the experimental data. These parameters can describe the material behaviour from damage initiation to failure or macrolevel rupture in the structure.
5. The proposed model accurately captures the tensile behaviour of the epoxy material. A similar model for shear and compressive behaviour can be developed. Thus, these can be used to predict the overall behaviour of the epoxy material.

Acknowledgements Authors thank technical staff of Aeromodeling Lab and Structures lab from Department of Aerospace Engineering, Indian Institute of Technology Kanpur, India for helping in the development of molds and materials.

References

1. Kachanov, L.: Time of the rupture process under creep conditions. Isv. Akad. Nauk. SSR. Otd Tekh. Nauk **8**, 26–31 (1958)
2. Rabotnov, Y.N.: Creep Rupture, in: Applied mechanics, pp. 342–349. Springer, Berlin (1969)
3. Chaboche, J.-L.: Continuous damage mechanics—a tool to describe phenomena before crack initiation. Nuclear Eng. Des. **64**(2), 233–247 (1981)
4. Janson, J.: Damage model of crack growth and instability. Eng. Fract. Mech. **10**(4), 795–806 (1978)
5. Mazars, J., Pijaudier-Cabot, G.: From damage to fracture mechanics and conversely: a combined approach. Int. J. Solids Struct. **33**(20), 3327–3342 (1996)
6. Daudeville, L., Allix, O., Ladeveze, P.: Delamination analysis by damage mechanics: some applications. Compos. Eng. **5**(1), 17–24 (1995)
7. Allix, O., Leveque, D., Perret, L.: Identification and forecast of delamination in composite laminates by an interlaminar interface model. Compos. Sci. Technol. **58**(5), 671–678 (1998)
8. Ladevèze, P., Allix, O., Gornet, L., Lévêque, D., Perret, L.: A computational damage mechanics approach for laminates: identification and comparison with experimental results. Stud. Appl. Mech. **46**, 481–500 (1998)
9. Ladeveze, P., Allix, O., Daudeville, L.: Mesomodeling of Damage for Laminate Composites: Application to Delamination, in: Inelastic Deformation of Composite Materials. Springer, New York (1991)
10. Ladevèze, P., Lubineau, G.: On a damage mesomodel for laminates: micro–meso relationships, possibilities and limits. Compos. Sci. Technol. **61**(15), 2149–2158 (2001)
11. Hill, R.: Elastic properties of reinforced solids: some theoretical principles. J. Mech. Phys. Solids **11**(5), 357–372 (1963)
12. Hill, R.: Theory of mechanical properties of fibre-strengthened materials: I. Elastic behaviour. J. Mech. Phys. Solids **12**(4), 199–212 (1964)
13. Dassault Systèmes.: Abaqus 6.10 online documentation. Dassault Systèmes, Providence, Rhode Island (2010)
14. Hibbitte, K.: Abaqus user subroutines reference manual. HKS INC (2005)
15. Allaoui, A., Bai, S., Cheng, H.-M., Bai, J.: Mechanical and electrical properties of a MWNT/epoxy composite. Compos. Sci. Technol. **62**(15), 1993–1998 (2002)
16. Schadler, L.S., Giannaris, S.C., Ajayan, P.M.: Load transfer in carbon nanotube epoxy composites. Appl. Phys. Lett. **73**(26), 3842–3844 (1998). doi:10.1063/1.122911. http://scitation.aip.org/content/aip/journal/apl/73/26/10.1063/1.122911
17. Gojny, F.H., Wichmann, M.H.G., Köpke, U., Fiedler, B., Schulte, K.: Carbon nanotube-reinforced epoxy-composites: enhanced stiffness and fracture toughness at low nanotube content. Compos. Sci. Technol. **64**(15) 2363–2371 (2004)
18. Alvarez, V., Valdez, M., Vzquez, A.: Dynamic mechanical properties and interphase fiber/matrix evaluation of unidirectional glass fiber/epoxy composites. Polym. Test.**22**(6), 611–615 (2003). doi:10.1016/S0142-9418(02)00164-2. http://www.sciencedirect.com/science/article/pii/S0142941802001642
19. Yang, B., Kozey, V., Adanur, S., Kumar, S.: Bending, compression, and shear behavior of woven glass fiber–epoxy composites. Compos. Part B Eng. **31**(8), 715–721 (2000). doi:10.1016/S1359-8368(99)00052-9. http://www.sciencedirect.com/science/article/pii/S1359836899000529
20. W. Goertzen, M. Kessler, Creep behavior of carbon fiber/epoxy matrix composites. Mater. Sci. Eng. A **421**(12) (2006) 217–225. In: Internal Stress and Thermo-Mechanical Behavior in Multi-component Materials Systems, (TMS) Annual Meeting, 2004. doi:10.1016/j.msea.2006.01.063. http://www.sciencedirect.com/science/article/pii/S0921509306001390
21. Dong, S., Gauvin, R.: Application of dynamic mechanical analysis for the study of the interfacial region in carbon fiber/epoxy composite materials. Polym. Compos. **14**(5), 414–420 (1993). doi:10.1002/pc.750140508
22. Choi, N., Kinloch, A., Williams, J.: Delamination fracture of multidirectional carbon-fiber/epoxy composites under mode i, mode ii and mixed-mode i/ii loading. J. Compos. Mater. **33**(1), 73–100 (1999)
23. Yokozeki, T., Aoki, Y., Ogasawara, T.: Experimental characterization of strength and damage resistance properties of thin-ply carbon fiber/toughened epoxy laminates. Compos. Struct. **82**(3), 382–389 (2008). doi:10.1016/j.compstruct.2007.01.015. http://www.sciencedirect.com/science/article/pii/S0263822307000219
24. Wang, X., Chung, D.D.L.: Short-carbon-fiber-reinforced epoxy as a piezoresistive strain sensor. Smart Mater. Struct. **4**(4), 363 (1995). http://stacks.iop.org/0964-1726/4/i=4/a=017
25. Wang, X., Chung, D.D.L.: Real-time monitoring of fatigue damage and dynamic strain in carbon fiber polymer-matrix composite by electrical resistance measurement. Smart Mater. Struct. **6**(4), 504 (1997). http://stacks.iop.org/0964-1726/6/i=4/a=017
26. Chevalier, J., Morelle, X., Bailly, C., Camanho, P., Pardoen, T., Lani, F.: Micro-mechanics based pressure dependent failure model for highly cross-linked epoxy resins. Eng. Fract. Mech. **158**, 1–12 (2016)
27. Thomas, G.K.: Progressive delamination in unidirectional composites. unpublished M.Tech. thesis (2013)
28. Suquet, P.: Elements of homogenization for inelastic solid mechanics. Homog. Tech. Compos. Media **272**, 193–278 (1987)
29. Herakovich, C.T.: Mechanics of fibrous composites. Wiley, New York (1998)
30. Ward, I.M., Sweeney, J.: Mechanical Properties of Solid Polymers. Wiley, Hoboken (2012)
31. Li, F., Pan, J.: Plane-stress crack-tip fields for pressure-sensitive dilatant materials. Eng. Fract. Mech. **35**(6), 1105–1116 (1990)
32. Chang, W., Pan, J.: Effects of yield surface shape and round-off vertex on crack-tip fields for pressure-sensitive materials. Int. J. Solids Struct. **34**(25), 3291–3320 (1997)
33. Hsu, S.-Y., Vogler, T., Kyriakides, S.: Inelastic behavior of an AS4/PEEK composite under combined transverse compression and shear. part ii: modeling. Int. J. Plast. **15**(8), 807–836 (1999)
34. Khan, A.S., Huang, S.: Continuum Theory of Plasticity. Wiley, Hoboken (1995)
35. Montazeri, A., Khavandi, A., Javadpour, J., Tcharkhtchi, A.: Viscoelastic properties of multi-walled carbon nanotube/epoxy composites using two different curing cycles. Mater. Des. **31**(7), 3383–3388 (2010)
36. ASTM D638: Standard Test Method for Tensile Properties of Plastics. American Society for Testing and Materials, Philadelphia (1998)

37. Davis, J.R.: Tensile Testing. ASM International, Ohino (2004)
38. Gilat, A., Goldberg, R.K., Roberts, G.D.: Strain rate sensitivity of epoxy resin in tensile and shear loading. J. Aerosp. Eng. **20**(2), 75–89 (2007)